



HAL
open science

Sequential sensor selection for the localization of acoustic sources by sparse Bayesian learning

Milan Courcoux-Caro, Charles Vanwynsberghe, Cédric Herzet, Alexandre Baussard

► **To cite this version:**

Milan Courcoux-Caro, Charles Vanwynsberghe, Cédric Herzet, Alexandre Baussard. Sequential sensor selection for the localization of acoustic sources by sparse Bayesian learning. *Journal of the Acoustical Society of America*, 2022, 152 (3), pp.1695-1708. 10.1121/10.0014001 . hal-03780626

HAL Id: hal-03780626

<https://hal.science/hal-03780626>

Submitted on 19 Sep 2022

HAL is a multi-disciplinary open access archive for the deposit and dissemination of scientific research documents, whether they are published or not. The documents may come from teaching and research institutions in France or abroad, or from public or private research centers.

L'archive ouverte pluridisciplinaire **HAL**, est destinée au dépôt et à la diffusion de documents scientifiques de niveau recherche, publiés ou non, émanant des établissements d'enseignement et de recherche français ou étrangers, des laboratoires publics ou privés.

Sequential sensor selection for the localization of acoustic sources by Sparse Bayesian Learning

Milan Courcoux-Caro,¹ Charles Vanwynsberghe,^{2, a)} Cédric Herzet,³ and Alexandre Baussard⁴

¹⁾ENSTA Bretagne, Lab-STICC UMR 6285 CNRS, 2 Rue François Verny, 29806 Brest Cedex 09, France.

²⁾Technology Innovation Institute, 9639 Masdar City, Abu Dhabi, United Arab Emirates.

³⁾INRIA centre Rennes-Bretagne Atlantique, 35000, Rennes, France.

⁴⁾Université de Technologie de Troyes - LIST3N, 12 rue Marie Curie, CS 42060, 10004 Troyes Cedex, France.

(Dated: August 2022)

This paper deals with the design of sensor arrays in the context involving the localization of a few number of acoustic sources. Sparse approximation is known to be effective to find the source locations, but it depends on different array characteristics such as the number of sensors and the array geometry. The present paper tackles this array design problem under the form of a sequential sensor selection procedure. The proposed method alternates between two steps. One step involves a source localization estimator, given a current set of measurement points, to obtain the estimation variance. Then the other step selects the new point where a future measurement will maximally decrease the variance from previous step. As such, the procedure can be applied *online*. Both numerical and experimental studies are conducted in an indoor nearfield configuration. Results show that the proposed approach performs better than offline state-of-the art methods, and the presented empirical study reveals a better robustness to the model mismatches originating from the room reflections.

[<https://doi.org/10.1121/10.0014001>]

[XYZ]

Pages: 1–15

I. INTRODUCTION

Source localization from a limited number of point-wise measurements is a common inverse problem in acoustic or radar applications. The literature exhibits a plethora of techniques to solve this problem. To name a few, it goes from methods of beamforming^{9,41}, deconvolution⁵, to estimators relying on the help of a prior through a Bayesian framework², or Compressed Sensing (CS) when there are few sources in the field⁴³.

However, irrespective of the chosen technique, the quality of source localization is impacted by the configuration of the array. To improve the reconstruction accuracy, the classical antenna theory suggests the trivial solution of increasing the number of sensors, placed at randomized positions to avoid a regular geometry structure. Such an approach remains valid, especially when the chosen method is sensitive to side and grating lobes – such as beamforming. However, in this context the randomization of sensor positions does not meet any form of optimality. Moreover, depending on the context, the number (resp. positions) of sensors may be constrained by cost (resp. structural) limitations.

An extensive literature depicts how to optimize the array geometry. One well-known approach relies on a refinement of the directivity pattern, such as the reduction of the side lobe levels^{3,44}. The geometry is obtained as a solution of a non-convex minimization problem, typically via a genetic algorithm^{20,28,30}, swarm optimization²⁶ or simulated annealing^{31,40}. This approach is popular and remains relevant to improve beamforming efficiency, since the latter is inherently related to the beampattern shape. However, it is not relevant for other methods than beamforming. For example in CS, the quality of sparse source localization depends on the incoherence of the acoustic propagation operator. In this case, the geometry is preferably designed based on a statistical approximation of the restricted isometry property, or the null space property¹⁴.

Finding an optimal array geometry can be tackled by ideas stemming from experimental design^{13,32}, and is known under the name of *sensor selection* in the literature. The goal is to minimize the variance of some estimator for a given number of sensors and a collection of candidate positions. Although attractive, acoustic array design by sensor selection seems less common than beampattern-based methods. One example, in⁷, illustrates an optimal array deployment for localization by time of arrival measurements. In¹⁸, the number of measurements is sequentially augmented by moving a microphone array to a new optimal position, and the source reconstruction is refined at each iteration. Despite being

^{a)}This work was also done while the author was affiliated at (a) SEACom team, LabISEN Yncrea Ouest, 20 Rue Cuirassé Bretagne CS 42807, 29228, Brest Cedex 2, France (b) ENSTA Bretagne, Lab-STICC UMR 6285 CNRS, 2 Rue François Verny, 29806 Brest Cedex 09, France; charles.vanwynsberghe@tii.ae

elegant, this approach is specific to spread sources due to the use of Gaussian prior.

The aim of the present work is to introduce a sequential sensor selection when there are few acoustic sources. It is derived from the Bayesian framework and relies on two key points. First it computes a solution of the source vector by a sparsity-enhancing hierarchical model⁴⁵. Second, it selects the next sensor position which maximally reduces the variance of the previously computed solution. With such a sequential procedure, the optimal selection is informed by the previous measurements²⁴, and successful applications were demonstrated such as in MRI³⁶ or temperature monitoring²⁷. The present work investigates the efficiency of the idea in acoustic source localization, with a validation in an experimental, nearfield indoor scenario. To the best of authors' knowledge, this is the first paper exhibiting *in situ* experiments of sensor selection applied to source localization with real data.

The paper is organized as follows. In sec. II, the theory of the proposed approach is described. The coupled problems of sensor selection and source localization are detailed, then the derivations to obtain a low-complexity greedy algorithm are presented in sec. III. Next, sec. IV defines the case of study: an indoor setup for acoustic source localization. After a description (in sec. V) of the chosen criterion and state-the-art methods to assess and compare the performance of the proposed algorithm, results from both simulated and experimental results are analyzed in sec. VI. Also, it includes a parametric study on the robustness of sensor selection to model mismatch induced by room reflections.

Notations used in this paper are as follows. Bold-face letters are reserved for matrices (uppercase) and vectors (lowercase), and standard font denotes scalar parameters. The symbol \cdot^T (resp. \cdot^H) defines the transpose (resp. Hermitian transpose) of a matrix, $\det(\mathbf{A})$ is the determinant of \mathbf{A} , $\text{diag}(\mathbf{a})$ is a diagonal matrix with the elements of \mathbf{a} on the diagonal. \mathbf{I}_N is the identity matrix of size $N \times N$, and $\mathbf{0}_N$ is the column vector with N zeros. The variable estimates are written with the $\tilde{\cdot}$ tilde symbol. Calligraphic letters \mathcal{K} (resp. \mathcal{M}) denote coordinate sets of cardinality $|\mathcal{K}|$ (resp. $|\mathcal{M}|$). Probabilities are defined as $P(\cdot)$ when they are discrete, and as $\mathcal{P}(\cdot)$ when they are density functions. Finally we denote $\mathcal{NC}(\mathbf{a}, \mathbf{A})$ the complex multivariate Normal distribution of mean \mathbf{a} and covariance \mathbf{A} , and the expectation operator is $\mathbb{E}\{\cdot\}$.

II. SENSOR SELECTION FOR SOURCE LOCALIZATION

A. Model description

Let the array of M sensors lie in the 3-dimensional space, with the m -th sensor position denoted $\mathbf{p}_m \in \mathbb{R}^3$. The set $\mathcal{M} = \{\mathbf{p}_1, \dots, \mathbf{p}_m, \dots, \mathbf{p}_M\}$ contains the sensor positions, meaning that $|\mathcal{M}| = M$.

The main goal of our work is to determine a subset $\mathcal{K} \subseteq \mathcal{M}$ of K sensor positions leading to good source-localization performance. We suppose that there are S sources at frequency f to localize, and we approximate

the continuous source domain by a grid of N points. Thus, we consider a linear on-grid model with additive noise to describe each measurement. For the m -th sensor the model writes:

$$y(\mathbf{p}_m) = \mathbf{a}(\mathbf{p}_m)\mathbf{s} + w_m, \quad (1)$$

with $\mathbf{s} \in \mathbb{C}^{N \times 1}$ the vector of unknown source amplitudes to be estimated, $\mathbf{a}(\mathbf{p}_m) \in \mathbb{C}^{1 \times N}$ the row vector describing the propagation of the sources from the grid to the sensor position \mathbf{p}_m at frequency f , and $w_m \in \mathcal{NC}(0, \sigma^2)$ is a random noise.

The acoustic field is supposed to contain a few number of sources, with the condition that $S \ll N$. Accordingly the signal \mathbf{s} is S -sparse, *i.e.* it has S non-zero elements. Note that there is no particular constraint on the propagation model, excepted linearity: the row vector $\mathbf{a}(\mathbf{p}_m)$ may depict conditions of far or near field, with or without specific boundary conditions depending on the field of application – *e.g.* indoor with multipaths or underwater in shallow water²³.

Let $\mathcal{K} \subseteq \mathcal{M}$ to be a subset of sensors from the array, meaning that $|\mathcal{K}| \leq M$. Defining the measurement vector as $\mathbf{y}_{\mathcal{K}} = [y(\mathbf{p}_1), \dots, y(\mathbf{p}_m), \dots, y(\mathbf{p}_{|\mathcal{K}|})]^T$, the model (1) in matrix form reads:

$$\mathbf{y}_{\mathcal{K}} = \mathbf{A}_{\mathcal{K}}\mathbf{s} + \mathbf{w}_{\mathcal{K}}, \quad (2)$$

with $\mathbf{A}_{\mathcal{K}} = [\mathbf{a}(\mathbf{p}_1)^T, \dots, \mathbf{a}(\mathbf{p}_m)^T, \dots, \mathbf{a}(\mathbf{p}_{|\mathcal{K}|})^T]^T$ the $|\mathcal{K}| \times N$ forward propagation matrix, and $\mathbf{w}_{\mathcal{K}} = [w_1, \dots, w_m, \dots, w_{|\mathcal{K}|}]^T$ the $|\mathcal{K}| \times 1$ noise vector. We assume that the elements of $\mathbf{w}_{\mathcal{K}}$ are independent and identically distributed: $\mathbf{w}_{\mathcal{K}} \sim \mathcal{NC}(\mathbf{0}_{|\mathcal{K}|}, \sigma^2 \mathbf{I}_{|\mathcal{K}|})$.

In this paper, we consider a Bayesian framework to devise our sensor-placement procedure. To this end, we need to define a prior model $\mathcal{P}(\mathbf{s})$ which properly accounts for the sparse nature of \mathbf{s} . A typical choice for $\mathcal{P}(\mathbf{s})$ is the so-called Bernoulli-Gaussian model (see *e.g.*^{21,22,35,38,46}). One standard formulation of this model reads:

$$\mathcal{P}(\mathbf{s}) = \prod_{n=1}^N \mathcal{P}(s_n), \quad (3)$$

with

$$\mathcal{P}(s_n) = \sum_{b_n \in \{0,1\}} \mathcal{P}(s_n|b_n)P(b_n). \quad (4)$$

$P(b_n) = \text{Ber}(p)$ is a Bernoulli distribution with parameter $p \in [0, 1]$ and $\mathcal{P}(s_n|b_n) = \mathcal{CN}(0, \sigma_{b_n}^2)$ is a zero-mean complex Gaussian density with variance $\sigma_{b_n}^2$. It can be easily seen that typical realizations of the model are (quasi-) sparse vectors when $p \sim 0$, $\sigma_0^2 \sim 0$ and $\sigma_1^2 \gg 0$. Interestingly, several authors (see^{21,38}) have emphasized the connection between a maximum a posteriori estimation problem involving a Bernoulli-Gaussian prior and the “ ℓ_0 -penalized” problem, ubiquitous in the field of sparse representations. The Bernoulli-Gaussian model

can thus be seen as an ideal probabilistic modelling of the sparse nature of the source vector \mathbf{s} .

In this work, we use the Bernoulli-Gaussian prior as a starting point to motivate our sensor-selection methodology. In the next sections, we will then consider some simplifications to circumvent the computational bottleneck induced by this model.

B. The sensor selection problem

In the context of source localization, the sensors must be positioned in such a way that the uncertainty in the number, positions and amplitudes of the sources is minimized when the measurements are collected. In the Bayesian framework considered in this paper, the uncertainty in these quantities is directly related to the spread of the posterior distribution $p(\mathbf{s}|\mathbf{y}_{\mathcal{K}})$. For instance, if $p(\mathbf{s}|\mathbf{y}_{\mathcal{K}})$ reduces to a Dirac's delta, \mathbf{s} can be perfectly recovered from $\mathbf{y}_{\mathcal{K}}$ and there is no residual uncertainty on the source locations upon the observation of $\mathbf{y}_{\mathcal{K}}$. Contrarily, when the mass of $p(\mathbf{s}|\mathbf{y}_{\mathcal{K}})$ is spread over the whole domain \mathbb{C}^N , the uncertainty about \mathbf{s} is high and the error made by any point-estimate $\hat{\mathbf{s}}_{\mathcal{K}}$ is likely to be large.

Since working with the full distribution $p(\mathbf{s}|\mathbf{y}_{\mathcal{K}})$ is an intractable task, it is common to map the latter to some scalar-valued cost function, see^{4,32}. In this paper, we use the following function:

$$f(\mathcal{K}) = \log \det(\boldsymbol{\Sigma}_{\mathcal{K}}), \quad (5)$$

where

$$\boldsymbol{\Sigma}_{\mathcal{K}} \triangleq \mathbb{E}_{\mathbf{s}|\mathbf{y}_{\mathcal{K}}} \{(\mathbf{s} - \mathbb{E}_{\mathbf{s}|\mathbf{y}_{\mathcal{K}}} \{\mathbf{s}\})(\mathbf{s} - \mathbb{E}_{\mathbf{s}|\mathbf{y}_{\mathcal{K}}} \{\mathbf{s}\})^H\} \quad (6)$$

is the covariance matrix of $\mathbf{s}|\mathbf{y}_{\mathcal{K}}$. This figure of merit is used in the so-called ‘‘D-optimal design’’ procedures and is widely known in the literature³². There are two motivations for using this function. First the covariance matrix fully describes the estimator variance, so a selection based on this matrix will naturally control the estimator uncertainty. Second, the covariance matrix describes the shape of the confidence ellipse in the N -dimensional space that contains the error estimation²⁵. The goal of the function is to capture the ellipse shape with one scalar. In D-optimality, the function $f(\mathcal{K})$ provides the log volume of this ellipse.

Note that relying on the covariance only has a limitation: it does not take the estimator bias into account. If the mean square error expression of the considered estimator exists, the optimal selection can be based on it so that both bias and variance are reduced – e.g. see³³. This direction is out of scope in this paper, because the mean square error is unknown. Thus, there is no guarantee of controlling the estimator bias via D-optimal design.

The main question addressed in the paper is as follows: which sensors in \mathcal{M} should we select in order to minimize $f(\mathcal{K})$ when $|\mathcal{K}| = K$? This question formally write as follows:

Problem 1 *Given a set of potential sensor positions \mathcal{M} and a number of sensors $K \leq M$, find the subset of sen-*

sor positions \mathcal{K} such that

$$\tilde{\mathcal{K}} = \arg \min_{\mathcal{K} \subseteq \mathcal{M}} f(\mathcal{K}) \quad \text{subject to } |\mathcal{K}| = K. \quad (7)$$

Unfortunately, solving this problem is an intractable task. Bottlenecks are located at two levels. First, (7) is a discrete-valued optimization problem and, in the current state of knowledge, there is no *polynomial-time* procedure able to solve it. Second, the evaluation of the cost function $f(\mathcal{K})$ is intractable because the Bernoulli-Gaussian prior induces a summation over the 2^N possible configurations of the Bernoulli variable when $p(\mathbf{s}|\mathbf{y}_{\mathcal{K}})$ has to be evaluated.

In the rest of this paper, we propose a methodology for sensor selection which circumvents these two bottlenecks by resorting to some approximations. In the next two subsections, we show that the posterior covariance matrix $\boldsymbol{\Sigma}_{\mathcal{K}}$ (and thus the cost function $f(\mathcal{K})$) can be efficiently evaluated when the prior model $\mathcal{P}(\mathbf{s})$ is relaxed to some hierarchical Gamma-Gaussian model. In section III, we consider a greedy procedure to compute an approximate solution of (7).

Our approach can thus be seen as a tractable procedure to compute an approximation of the solution of (7).

C. Posterior covariance with Gaussian prior model

As a starting point, let us focus on the structure of the posterior covariance matrix when considering a Gaussian prior model:

$$\mathcal{P}(\mathbf{s}|\boldsymbol{\alpha}) = \mathcal{CN}(\mathbf{0}, \text{diag}(\boldsymbol{\alpha})^{-1}), \quad (8)$$

where $\boldsymbol{\alpha} \in \mathbb{R}_+^N$ denotes the inverse-variance of each element of \mathbf{s} .⁷ In this case, it is well known that the posterior covariance $\boldsymbol{\Sigma}_{\mathcal{K}}$ takes the form²:

$$\boldsymbol{\Sigma}_{\mathcal{K}} = (\sigma^{-2} \mathbf{A}_{\mathcal{K}}^H \mathbf{A}_{\mathcal{K}} + \text{diag}(\boldsymbol{\alpha})^{-1})^{-1}. \quad (9)$$

We note that $\boldsymbol{\Sigma}_{\mathcal{K}}$ is well-defined even when the problem is underdetermined ($M < S$) or ill-posed. Moreover, it has a nice closed-form solution which makes it attractive for our sensor-placement problem (7).

Unfortunately, it is well-known that Gaussian model (8) does not promote sparse realizations. It is therefore a poor prior to account for the sparse nature of the source vector \mathbf{s} . In fact, the only way to enforce the n -th element of the source vector \mathbf{s} to be close to zero with high probability is to set $\alpha_n^{-1} \simeq 0$. If $\boldsymbol{\alpha}$ is user-provided, this means that the source locations should be known in advance to obtain a proper prior model on \mathbf{s} .

In the next section, we investigate a solution to benefit from the closed-form expression of the Gaussian posterior covariance matrix while accounting for the prior lack of knowledge of $\boldsymbol{\alpha}$.

D. Hierarchical Gamma-Gaussian prior model

In the previous section we emphasized that Gaussian prior models lead to desirable closed-form expressions of

the posterior covariance matrix. Unfortunately, this prior is only of practical relevance when the parameter vector α is properly tuned to account for the sought source positions \mathbf{s} . In this section, we circumvent this issue by: *i*) considering a Gaussian prior model on \mathbf{s} as in (8); *ii*) including α as an *unknown* quantity in our estimation problem. The rationale for this strategy is as follows: even if a proper choice for α is not known in advance, a relevant value for this parameter may be learned from the received observations.

More precisely, we consider the following steps. First, since we assume that α is an unknown quantity and we operate in a Bayesian context, we must define a prior model on α . In this work, we rely on the well-known hierarchical model of Sparse Bayesian Learning to enforce sparsity³⁹, and define the following prior:

$$\mathcal{P}(\alpha|\rho) = \prod_{n=1}^N \Gamma(\alpha_n|1, \rho), \quad (10)$$

where $\Gamma(\alpha_n|1, \rho)$ denotes a Gamma distribution with shape parameters 1 and ρ . We set $\rho \gg 1$ which leads to a “flat” distribution, making all the values of α a priori roughly equally probable – see for example⁴⁵. We note that combining (8) and (10) is tantamount to defining a “Gaussian-Gamma” hierarchical prior model on (\mathbf{s}, α) . Here, the benefit from such a prior is that it is non-informative.

Second, we compute a maximum a posteriori estimate of α , *i.e.*,

$$\tilde{\alpha}_{\mathcal{K}} = \arg \max_{\alpha \in \mathbb{R}^+} \mathcal{P}(\alpha|\mathbf{y}_{\mathcal{K}}). \quad (11)$$

We note that problem (11) with a “Gaussian-Gamma” prior model has already been considered in the context of sparse representations (see³⁹) and source localization^{17,45}. In particular, it was emphasized that the solutions of (11) typically contain a few large components and many close-to-zero elements. This is in good agreement with our target problem where one searches to turn on only the elements of α corresponding to emitting sources. A numerical procedure, dubbed “Sparse Bayesian Learning” (SBL), instantiating the recursion of an “expectation-maximization” algorithm to problem (11) was also proposed in³⁹. We will consider this algorithm to compute $\tilde{\alpha}_{\mathcal{K}}$ and refer the reader to⁴⁵ for implementation details.

Third, we approximate the posterior covariance matrix by conditioning on $\alpha = \tilde{\alpha}_{\mathcal{K}}$:

$$\Sigma_{\mathcal{K}} \simeq \mathbf{E}_{\mathbf{s}|\mathbf{y}_{\mathcal{K}}, \tilde{\alpha}_{\mathcal{K}}} \{(\mathbf{s} - \mathbf{E}_{\mathbf{s}|\mathbf{y}_{\mathcal{K}}, \tilde{\alpha}_{\mathcal{K}}} \{\mathbf{s}\})(\mathbf{s} - \mathbf{E}_{\mathbf{s}|\mathbf{y}_{\mathcal{K}}, \tilde{\alpha}_{\mathcal{K}}} \{\mathbf{s}\})^H\}.$$

Interestingly, if the value of α is given, the prior model becomes Gaussian and one recovers the expression of the posterior covariance matrix given in (9), that is

$$\Sigma_{\mathcal{K}} \simeq (\sigma^{-2} \mathbf{A}_{\mathcal{K}}^H \mathbf{A}_{\mathcal{K}} + \text{diag}(\tilde{\alpha}_{\mathcal{K}})^{-1})^{-1}. \quad (12)$$

We note that the only difference between (9) and (12) is that the unknown parameter α has been replaced by

the posterior estimate $\tilde{\alpha}_{\mathcal{K}}$. We therefore recover the nice analytical expression of the covariance matrix obtained in the case of a Gaussian prior model but with a value of the parameter α estimated from $\mathbf{y}_{\mathcal{K}}$.

Towards a data-informed sensor selection

We remark that SBL is particularly attractive because the computed covariance is *learned* posterior to the sensor readings. Indeed, SBL helps to go towards a sensor selection strategy that is driven by both the model and the measured data, because $\tilde{\alpha}_{\mathcal{K}}$ is computed posterior to $\mathbf{y}_{\mathcal{K}}$.

From this key point, the next section proposes a data-informed sensor selection method, based on an iterative procedure.

III. DATA-INFORMED SENSOR SELECTION: A GREEDY ITERATIVE ALGORITHM

Problem 1 is combinatorial and is therefore not tractable with a high-dimensional sensor set \mathcal{M} . For applicability to large-scale arrays, we choose to follow a greedy heuristic approximating the solution. There are two motivations:

1. taken together the steps of selection have a low complexity in $\mathcal{O}(KMN^2)$ – justified below,
2. the framework is naturally *online* and data-informed, since each iteration allows to take the measurement from the new selected sensor into account.

Accordingly, the algorithm achieves a sequential design, and increments the size of \mathcal{K} until $|\mathcal{K}| = K$.

A. The “one-sensor” problem

Assume one wishes to add *one* extra sensor to a subset $\mathcal{K} \subseteq \mathcal{M}$. In the spirit of (7), it seems reasonable to select the sensor leading to the maximum decrease of cost function f , that is

$$\tilde{\mathbf{p}} = \arg \max_{\mathbf{p} \in \mathcal{M} \setminus \mathcal{K}} f(\mathcal{K}) - f(\mathcal{K} \cup \mathbf{p}). \quad (13)$$

In this section, we show that using covariance-matrix surrogate (12) with an additional approximation leads to a tractable analytical solution to this problem.

Let the function $f(\mathcal{K})$ be

$$f(\mathcal{K}) = \log \det(\Sigma_{\mathcal{K}}) \quad \text{with} \quad (14)$$

$$\Sigma_{\mathcal{K}} = (\sigma^{-2} \mathbf{A}_{\mathcal{K}}^H \mathbf{A}_{\mathcal{K}} + \text{diag}(\tilde{\alpha}_{\mathcal{K}})^{-1})^{-1}, \quad (15)$$

where $\tilde{\alpha}_{\mathcal{K}}$ is the solution of (11). With these definitions, a brute-force evaluation of (13) turns out to be computationally intensive since it requires to evaluate $\tilde{\alpha}_{\mathcal{K} \cup \mathbf{p}}$ for any $\mathbf{p} \in \mathcal{M} \setminus \mathcal{K}$. To improve the computational efficiency of our proposed method, we consider hereafter the following additional approximation:

$$\forall \mathbf{p} \in \mathcal{M} \setminus \mathcal{K} : \tilde{\alpha}_{\mathcal{K} \cup \mathbf{p}} \approx \tilde{\alpha}_{\mathcal{K}}. \quad (16)$$

The key point of this approximation is to access a tractable computation of the new covariance $\Sigma_{\mathcal{K} \cup \mathbf{p}}$ with an hypothetical additional sensor, without the explicit need of the new measurement $y(\mathbf{p})$ inside the expression. As a result, this leads to

$$\begin{aligned} \Sigma_{\mathcal{K} \cup \mathbf{p}}^{-1} &= \sigma^2 \mathbf{A}_{\mathcal{K} \cup \mathbf{p}}^H \mathbf{A}_{\mathcal{K} \cup \mathbf{p}} + \text{diag}(\tilde{\alpha}_{\mathcal{K} \cup \mathbf{p}})^{-1} \\ &\approx \sigma^2 \mathbf{A}_{\mathcal{K} \cup \mathbf{p}}^H \mathbf{A}_{\mathcal{K} \cup \mathbf{p}} + \text{diag}(\tilde{\alpha}_{\mathcal{K}})^{-1} \\ &= \sigma^2 \mathbf{A}_{\mathcal{K}}^H \mathbf{A}_{\mathcal{K}} + \text{diag}(\tilde{\alpha}_{\mathcal{K}})^{-1} + \tilde{\sigma}_{\mathcal{K}}^{-2} \mathbf{a}(\mathbf{p})^H \mathbf{a}(\mathbf{p}) \\ &= \Sigma_{\mathcal{K}}^{-1} + \sigma^2 \mathbf{a}(\mathbf{p})^H \mathbf{a}(\mathbf{p}). \end{aligned} \quad (17)$$

Using the “matrix determinant” lemma¹², we obtain

$$\det(\Sigma_{\mathcal{K}}) \approx \det(\Sigma_{\mathcal{K} \cup \mathbf{p}}) (1 + \sigma^2 \mathbf{a}(\mathbf{p}) \Sigma_{\mathcal{K}} \mathbf{a}(\mathbf{p})^H). \quad (18)$$

Finally, plugging this expression into (13), we end up with the following simplified optimization problem:

$$\tilde{\mathbf{p}} = \arg \max_{\mathbf{p} \in \mathcal{M} \setminus \mathcal{K}} \log (1 + \sigma^2 \mathbf{a}(\mathbf{p}) \Sigma_{\mathcal{K}} \mathbf{a}(\mathbf{p})^H). \quad (19)$$

Note that this sequential form of D-optimal design was derived by Wynn *et al* in⁴² in the case of linear models. Through this form, computing the log volume reduction is efficient as it requires $\mathcal{O}(N^2)$ operations to score the function for each candidate (once $\Sigma_{\mathcal{K}}$ has been evaluated).

B. Remarks and connections with related literature

Remark 1 The eq. (19) was also derived by information-theoretical tools³⁷. It helps to understand its optimality as a choice of the most informative sensor. The differential entropy, by definition, describes the entropy of a random variable admitting a distribution with respect to the Lebesgue measure. In the considered hierarchical model for SBL with measurements from \mathcal{K} , the conditional probability density function $\mathcal{P}(\mathbf{s} | \mathbf{y}_{\mathcal{K}}, \tilde{\alpha}_{\mathcal{K}})$ is a multivariate complex Gaussian distribution. In this case, the differential entropy writes: Applied to the multivariate normal posterior distribution of \mathbf{s} in SBL with measurements in \mathcal{K} , it writes:

$$\begin{aligned} h_{\mathcal{K}} &= - \int_{\mathbb{C}^N} f(\mathbf{s}) \log f(\mathbf{s}) d\mathbf{s}, \\ \text{with } f(\mathbf{s}) &= \frac{e^{(\mathbf{s} - \tilde{\mathbf{s}}_{\mathcal{K}})^H \Sigma_{\mathcal{K}}^{-1} (\mathbf{s} - \tilde{\mathbf{s}}_{\mathcal{K}})}}{\pi \det(\Sigma_{\mathcal{K}})}. \end{aligned} \quad (20)$$

In this case, it is well known that⁸ (Ch. 8):

$$h_{\mathcal{K}} \equiv \log \det(\Sigma_{\mathcal{K}}), \quad (21)$$

where \equiv means equality up to a constant. According to the same guideline, the differential entropy with one extra sensor amounts to $h_{\mathcal{K} \cup \mathbf{p}} \equiv \log \det(\Sigma_{\mathcal{K} \cup \mathbf{p}})$. As a result, the score in eq. (13) also amounts to the reduction of entropy $h_{\mathcal{K}} - h_{\mathcal{K} \cup \mathbf{p}}$, *i.e.* the information gained thanks to a sensor reading at \mathbf{p} . With the help of approximation in eq. (16), the information gain nearly equals the eq. (19).

Remark 2 One geometric interpretation of the constrained log volume reduction is the following. Supposing that the row norm $\|\mathbf{a}(\mathbf{p})\|$ is invariant, we search the direction in \mathbb{C}^N colinear to the major radius of $\Sigma_{\mathcal{K}}$, under the constraint that $\mathbf{a}(\mathbf{p})$ belongs to the manifold structured by the physical model. Note that, according to²⁴, if \mathbf{a} lies in $\mathbb{C}^{1 \times N}$ without any physical constraint, (i) it is not function of \mathbf{p} , and (ii) it maximizes the log volume reduction when it is equal to the eigenvector paired with the largest eigenvalue of $\Sigma_{\mathcal{K}}$.

C. Final algorithm

As a whole, the proposed method is an online greedy sensor selection. Based on the covariance a posteriori from SBL, it is naturally data-informed. Note that it inherently calls SBL, so the selection jointly performs an online source localization. Indeed, the source vector $\tilde{\mathbf{s}}_{\mathcal{K}}$ can be estimated based as a function of $\Sigma_{\mathcal{K}}$ as:

$$\tilde{\mathbf{s}}_{\mathcal{K}} = \Sigma_{\mathcal{K}} \mathbf{A}_{\mathcal{K}}^H \mathbf{y}_{\mathcal{K}}. \quad (22)$$

The method is summarized in the algorithm 1.

Input : $\mathcal{K} = \emptyset, K, \mathcal{M}, \mathbf{y}_{\mathcal{M}}$

Output: \mathcal{K} with $|\mathcal{K}| = K$

Initialize : take $\mathbf{p}_k, \mathbf{p}_l \in \mathcal{M}$ randomly, and initialize $\mathcal{K} = \{\mathbf{p}_k, \mathbf{p}_l\}$;

while $|\mathcal{K}| < K$ **do**

 Estimate $\Sigma_{\mathcal{K}}$ via eqs (11) and (12) ;

 Find $\tilde{\mathbf{p}} = \arg \max_{\mathbf{p} \in \mathcal{M} \setminus \mathcal{K}} 1 + \sigma^{-2} \mathbf{a}(\mathbf{p}) \Sigma_{\mathcal{K}} \mathbf{a}(\mathbf{p})^H$;

$\mathcal{K} \leftarrow \mathcal{K} \cup \tilde{\mathbf{p}}$;

end

ALGORITHM 1: Greedy algorithm for data-informed and online sensor selection.

Note that an initialization step is necessary: \mathcal{K} cannot be empty in the present case, since SBL needs data, including at the first iteration. One initial sensor is enough in theory, but not enough to extract a spatial information on the source field with SBL. Thus, two initial sensors are picked at random and included in \mathcal{K} .

The selection step requires an extensive search on $M - |\mathcal{K}|$ candidates: the computation cost *slightly* reduces as \mathcal{K} is growing in size. An upper bound in complexity of this step is $\mathcal{O}(MN^2)$, and $\mathcal{O}(KMN^2)$ for the selection of K sensors accordingly.

IV. CASE OF STUDY: INDOOR SOURCE LOCALIZATION

This paper illustrates the method of sensor selection with an application to the near-field acoustic source localization indoor. Experiments *in situ* are performed in a room equipped with a very large array. All the numerical and experimental results below follow the same common configuration, described in the next section.

A. Experimental scenario: a 1020-microphone array mounted on walls

The room and the antenna hardware are fully described in^{10,11}. The picture in fig. 1 shows the global setup during an acquisition. The array is made up of $M = 1020$ digital MEMS microphones, and is supported by the walls of the room of shape $8.01\text{m} \times 3.75\text{m} \times 2.94\text{m}$. The sensor positions \mathbf{p}_m on these walls are random, as illustrated in fig. 2(a). To ensure a tractable source localization, the source field domain is restricted to the horizontal plane highlighted by the red laser in fig. 1. The height of this plane is 1.35 m, and the acoustic sources (cf. the blue speaker, upper right) are positioned in the plane thanks to the laser level.

An acquisition set is created at a sampling frequency of 25 kHz, for 25 source positions plotted with red points in fig. 2(b). Each acquisition contains one single source in emission. In this way, it is easy to create flexible source field configurations by summing each of these acquisitions at will. The underlying motivation is to enable to do Monte Carlo simulations on real data.

The source is assumed to be omni-directional and pointwise. At each acquisition, the speaker emits a sinusoidal component at the frequency $f = 500$ Hz. The x- and y-axis true source positions are measured in reference to two vertical walls with as laser tape. To turn the source localization in the harmonic form, discrete Fourier transforms are made on frames of 6250 time samples (*i.e.* 0.25 s), to extract the chosen frequency from them.

B. Propagation model indoor and model mismatch

As a starting point, let us recall how to write the propagation model in a near and free fields:

$$[\mathbf{a}(\mathbf{p}_m)]_n = \frac{1}{\|\mathbf{p}_m - \mathbf{r}_n\|_2} e^{-i \frac{2\pi f}{c_0} \|\mathbf{p}_m - \mathbf{r}_n\|_2}, \quad (23)$$

where f is the frequency in Hz, c_0 the sound speed in m/s, and \mathbf{r}_n the position of the n -th source on the grid. Obviously, such a model is mismatched indoor. It can be refined, by taking the presence of walls into account.

Reflections from the 6 surfaces (*i.e.* the 4 walls, ceiling and ground) are integrated to the model with the method of image sources¹. To do so, each point of the original source grid is duplicated with respect to the surface positions, as depicted in fig. 3. The number of mirrored points depend on the chosen order of reflection. For instance, a model with reflections:

- of the first order needs the purple duplicates in fig. 3(b);
- of the second order needs both purple and red duplicates.

The image source method is convenient, because it is linear and its analytical expression is easily calculable. Indeed, the general form of its related propagation model

can be written as^{1,34}:

$$[\mathbf{a}(\mathbf{p}_m)]_n = \frac{1}{\|\mathbf{p}_m - \mathbf{r}_n\|_2} e^{-i \frac{2\pi f}{c_0} \|\mathbf{p}_m - \mathbf{r}_n\|_2} + \sum_{j=1}^J \beta_j \frac{1}{\|\mathbf{p}_m - \mathbf{r}_n^j\|_2} e^{-i \frac{2\pi f}{c_0} \|\mathbf{p}_m - \mathbf{r}_n^j\|_2}, \quad (24)$$

with J the total number of effective reflections, \mathbf{r}_n^j the position of the j -th image source corresponding to the original source point \mathbf{r}_n , and β_j each effective attenuation coefficient.

We assume that the absorption by the walls does not induce any phase shift, and does not depend on the wave incidence angle. So β_j are real constant numbers for each index j . The reflection coefficients are roughly estimated by finding a high correlation between the measurements and synthesized data. We fix $\beta_j = 0.75$ for the ceiling and walls, and $\beta_j = 0.5$ for the ground as coefficients of the first order. Other coefficients of the z -th order are derived accordingly, by taking into account the appropriate reflections occurring in the acoustic path. By awareness, we verified that small variations of β_j lead in marginal impacts on the provided results in sec. VI.

The addressed model (24) will be used to approximate the indoor propagation but obviously the level of approximation will introduce model mismatches, the free-field model (23) being the coarsest choice. Nevertheless, promising works show that SBL is robust to mismatches because of its adaptive nature that results from the underlying probabilistic model^{15,16}. To follow up on this work, the experiments in sec. VI will analyze if the data-informed sensor selection leverages this adaptive nature to enhance the localization accuracy.

V. EVALUATION SETUP OF THE PERFORMANCE

In this section we briefly introduce the state-of-the-art methods used as references to evaluate the performances of the proposed approach. Before that, we define the criterion used for the comparison.

A. Evaluation criterion

To compare the performances of the proposed method against the state-of-the-art ones (described below), we propose to use the following criterion: once the antenna array has been selected for a given number of sensors, the SBL is used to provide the complex source vector $\tilde{\mathbf{s}}_{\mathcal{K}}$ (22) on the grid. Note that our approach inherently involves the SBL computation online.

Starting from the prior knowledge that we have S sources, we select the S highest peaks from the absolute value of $\tilde{\mathbf{s}}_{\mathcal{K}}$ elements (the SBL doesn't necessarily gives spikes, that is why we look for the positions of the local maxima). Then, we compute the euclidean distance between the true source positions and these positions. If this distance is lower than some given radius threshold, then we consider that the estimated source location is a true positive. Let N_{tp} be the number of true positives.

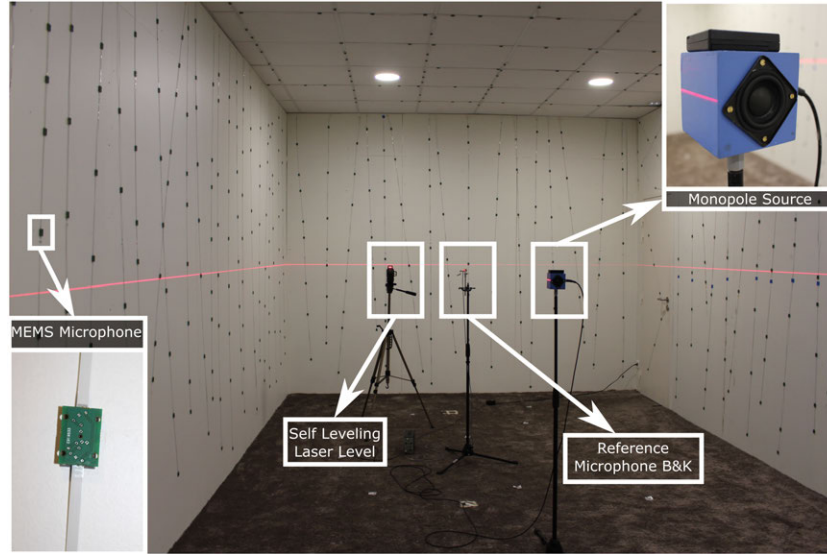


FIG. 1. Experimental setup indoor: 1020 microphones mounted on walls. (color online)

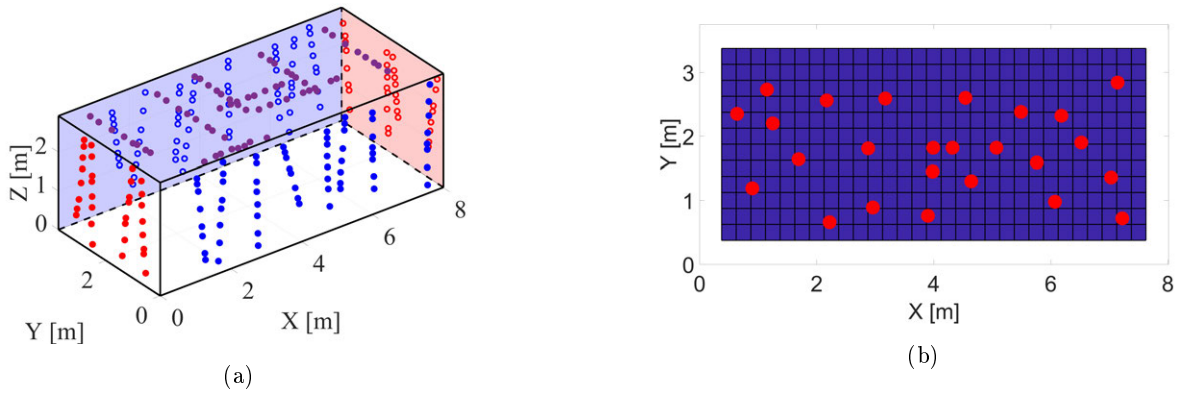


FIG. 2. (a) Sensor positions on the walls. For a better visibility only 256 of the 1020 sensors are shown, filled points for front walls and hollow points for back walls, and different colors for each wall are used. (b) Positions of the 25 sources (red dots) in the room measured with a laser. The height of the sources is 1.35 meters. The grid, represented in blue, does not cover the space up to the walls. A gap of 50cm between the grid and these walls was preserved in order to avoid areas with possibly strong reflections. (color online)

Moreover, since we are going to achieve Monte Carlo simulations with N_r realizations, the result will be displayed as empirical mean of true positives in percent:

$$\text{True positive} = \frac{100}{N_r} \sum_{i=1}^{N_r} \frac{N_{tp,i}}{S} [\%], \quad (25)$$

where i stands for the index of the Monte Carlo realization. In addition, the Jaccard index will be plotted because it also takes False positives and False negatives

into account. We recall, from its expression

$$\begin{aligned} &\text{Jaccard index} \\ &= \frac{\text{True positive}}{\text{True positive} + \text{False positive} + \text{False negative}}, \end{aligned} \quad (26)$$

that it takes values from 0 (poor performance) to 1 (best performance).

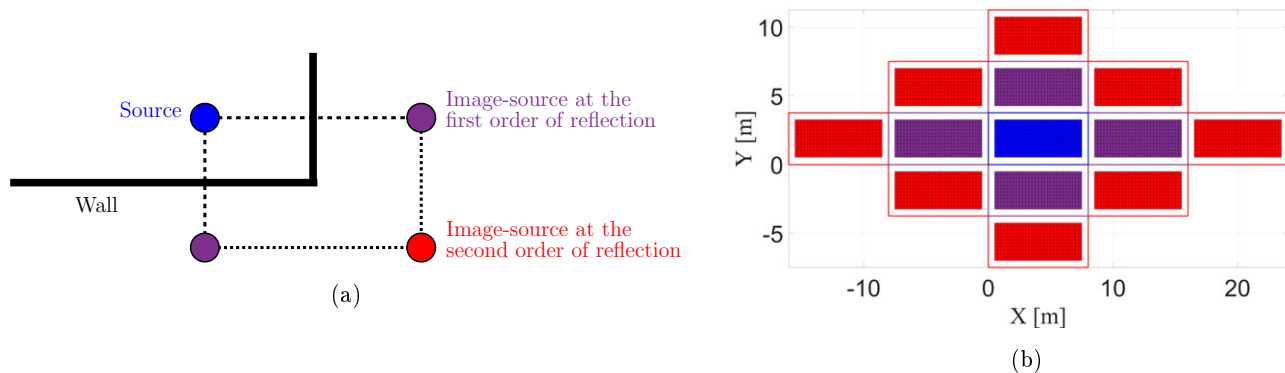


FIG. 3. (a) Schema of the image-source model used to take into account the reflections. The blue dot corresponds to the source position, the magenta dots are the first-order positions, and the red dot is the second-order position. (b) The different discretized spaces in 2 dimension created up to the second order of reflections. The blue space is the initial room, the magenta space is the first order and red the second order. A 50cm gap was preserved between walls and the source grid. (color online)

B. State-of-the-art approaches

We propose to compare our sensor selection strategy with three common approaches: (a) random selection, (b) array synthesis based on beampattern optimization by a genetic algorithm, and (c) a method based on convex relaxation and the Fisher information matrix. We describe below these methods, and the required adjustments to perform the comparison properly.

1. Random selection (*SelRand*)

Since our approach is based on the sparsity prior, it seems appropriate to consider solutions from the CS literature. In this framework, making random linear measurements of sparse vectors is known to be effective to obtain good reconstruction guarantees. However, in the present acoustic problem, the matrix $\mathbf{A}_{\mathcal{K}}$ is deterministic and its elements can not deliberately randomized. But studies show that the requirements from the CS framework can be approximated by selecting the sensor positions at random^{6,43}.

To compare this strategy with the proposed approach, we simply replace in Algorithm 1 the optimal selection $\tilde{\mathbf{p}}$ by a uniform random selection in the set $\mathcal{M} \setminus \mathcal{K}$. We still compute SBL at each iteration though, in order evaluate the approach according to the (increasing) number of selected sensors.

2. Beampattern optimization with genetic algorithm (*SelGen*)

Array design can be achieved by an optimization problem seeking to reduce – most of the time – the Maximum Sidelobe Level (MSL) of the beampatterns²⁰. Shortly, the goal is to maximize the difference between the main lobe and the sidelobe levels. This kind of approach is especially relevant for source localization using beamforming. The optimization problem, which is non-

convex, can be solved using several approaches. In this paper, we use the MSL-based beampattern optimization based on a genetic algorithm proposed in²⁸. Once the array is designed for a given number of sensors, we perform SBL and get the evaluation criterion (25).

Note that this method is offline, and not inherently iterative. So, to compare with the online sequential selections, the arrays are independently designed for different values of K . Finally, because the present experimental setup is different from the one in²⁸, some adjustments should be done regarding the initial choice of three parameters: the number of generations, of individuals, and the mutation coefficient – numerical values are given in section VI.

3. Convex relaxation with the Fisher information matrix (*SelRelax*)

The last method considered in this paper is the one proposed in⁷. The goal of this method is to select the positions of a given number of sensors by maximizing the smallest eigenvalue of the Fisher Information Matrix (FIM) via convex relaxation. Note that maximizing the smallest FIM eigenvalue is known as E-optimal design. In the article, Chepuri *et al* illustrate their studies with a source localization scenario based on time of arrival measurements. Since we use a different model, two key adjustments should be emphasized for a proper implementation.

First, the problem must be overdetermined: the number of unknowns must be smaller than the number of sensors K . As such the linearized model (2) is not convenient when the source grid size N is large. As explained in⁷, it is tackled by staying with the continuous nonlinear form of the propagation model, and calculating the analytic FIM with 5 scalar parameters: the x- and y-coordinates of the source position, the source amplitude and phase, and σ^2 . It leads to a FIM of size 5×5 . This

choice of variables inherently describes the presence of only one source in the field.

Therefore, as the second key point, Chepuri *et al* develop an idea to discretize the domain of values potentially taken by the 5 parameters, while preserving the same overdetermined form. To do so, the relaxation problem replaces the use of a FIM by the use of a block diagonal matrix; each block is one FIM computed with a set of parameter values⁷ (Sec. III.a). We use CVX toolbox¹⁹ to solve the relaxed problem. To keep the computation tractable, the parameter domain discretization should be coarse because the size of the block diagonal matrix quickly grows. Among the 5 scalar parameters, we only discretize the x- and y-coordinate parameters at the 25 true source positions. It leads to a block diagonal matrix with $5 \times 25 = 125$ rows and columns.

This method is model-informed only and, more importantly, is not sequential *de facto* – like the method in sec. VB2. Thus, we proceed in the same way by designing the arrays independently for different values of K .

VI. RESULTS

In this section we present results exploiting both simulated and experimental data, in the scenario of source localization indoor in near field, thoroughly described in sec.IV. Two main analyses are conducted: the effect of model mismatch and the performance evaluation of the proposed procedure against state-of-the-art approaches (c.f. section VB).

For the effect of model mismatch, we focus on how the steering matrix \mathbf{A}_K is defined regarding the reverberation. Based on the defined model in sec. IVB, we evaluate the difference of performances of source localization indoor, when the model either is free field (as eq. (23)), or takes reflections into account (as eq. (24)).

Concerning the implementation of the offline algorithms SelGen and SelRelax, described in sections VB2 and VB3, arrays are designed for K starting from 50 with a step of 50, and stopping at 1000 and 650, respectively. Note that the latter is stopped early because the convex optimisation by CVX fails beyond. Finally, some parameters of the genetic algorithm (SelGen) from²⁸ are adjusted: the number of generations and individuals are higher (250 against 100) and the mutation coefficient is lower (0.0001 against 0.01).

A. Results from numerical studies

We generate a set of $N_r = 300$ realizations by randomly selecting $S = 4$ source positions of the 25 plotted in fig.2(b). The plane containing the sources is discretized to create a grid of 29×12 points separated by 25 cm along x and y axes, leading to $N = 348$. Consequently, to compute the performance metric (25) the radius threshold deciding whether the localization is a true positive or not is fixed to 25 cm.

To simulate a scenario indoor, the data is synthesized with the mirror source model, and a reflection of the 3-rd order. Then, to evaluate the effect of the model mismatch, \mathbf{A}_K is build by still considering a source-mirror model, with reflections ranging from the 3-rd to the 0-th order.

The fig. 4(a) plots results without model mismatch, *i.e.* with the 3-rd order of reflection. All methods quickly reach 100% of true positives when the number of sensors increases. One can note that our approach is slightly better than the others, and SelRelax is the least good.

When the reflection order decreases (fig. 4(b), 4(c) and 4(d)), the model mismatch increases naturally, the performances degrade accordingly. One can note that our approach appears to be the less impacted, whereas SelGen and SelRelax seem to be the most sensitive to the mismatch. Also note that if the model error is too important (0-th reflection order, *i.e.* free field model), all methods performance are heavily impacted.

To complete the analysis via the True positive rate, the fig. 5 plots the Jaccard index. It focuses on the proposed method and the random selection, as these are the two top performing methods according to fig. 4. Both indicators have relatively similar trends, although the Jaccard index is slightly lower than the True positive with 0-th and 1-st reflection orders in the model. In these two cases the difference reveals the presence of False negatives and False positives.

From these studies, we may stipulate that our approach is more robust to model errors because it is the only data-informed method.

B. Results from experiments

For sake of comparison, we proceed with the same performance analysis as in previous simulations: methods are compared as a function of the number of sensors K , and the order of reflections. The $N_r = 300$ realizations for the Monte Carlo study are obtained based on the experimental setup described previously in sec. IVA.

The main difference with sec.VIA is that we do not know how many reflections are relevant to accurately model the received signal. One way to evaluate the order of reflections is to compute the correlation coefficient between the experimental and the synthesized data, based on the same configuration. The table I provides the average of theses coefficients over the 25 available positions of the source, as a function of the reflection order.

reflection order	0	1	2	3	4
correlation coefficient	0.43	0.58	0.69	0.68	0.61

TABLE I. Correlation coefficient between the experimental and the synthesized data, averaged on the 25 available source positions.

As expected, increasing the order in the synthesized data leads to a higher correlation coefficient, meaning

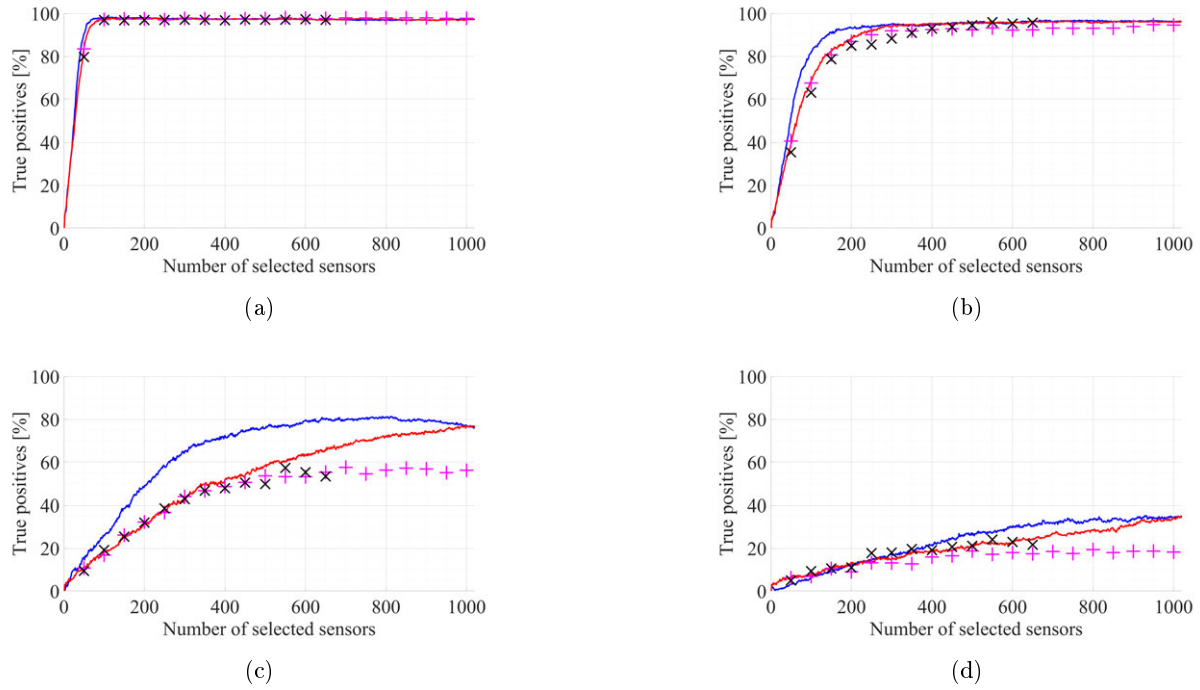


FIG. 4. Average percentage of true positives according to the number of sensors for our approach (blue line), SelRand (red line), SelGen (magenta plus) and SelRelax (black crosses). The data is synthesized with a 3-rd reflection order and $\mathbf{A}_{\mathcal{K}}$ is defined for reflection of the (a) 3-rd, (b) 2-nd, (c) 1-st and (d) 0-th order. (color online)

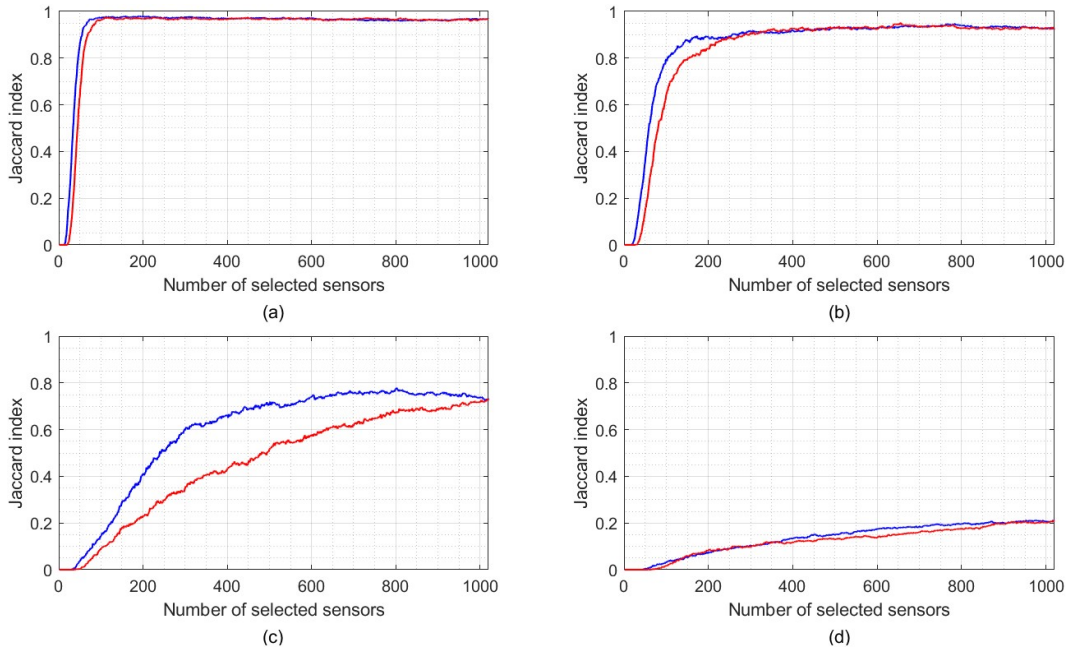


FIG. 5. Jaccard index according to the number of sensors for our approach (blue line) and SelRand (red line). $\mathbf{A}_{\mathcal{K}}$ is defined for reflection of the (a) 3-rd, (b) 2-nd, (c) 1-st and (d) 0-th order. (color online)

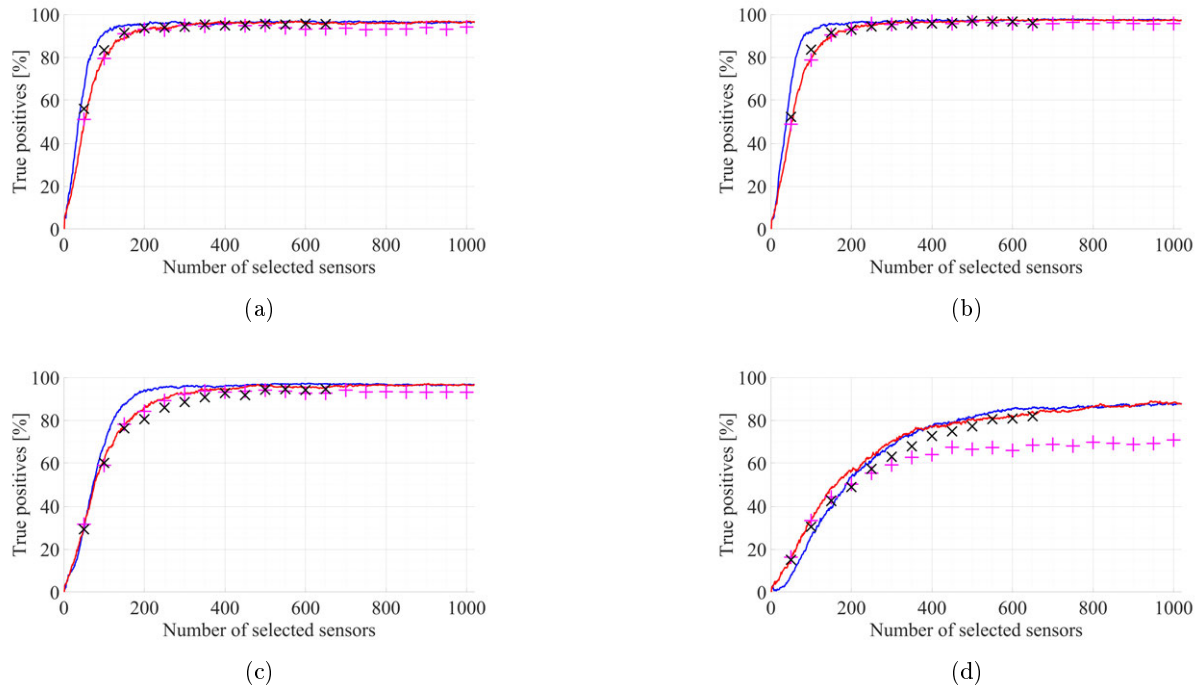


FIG. 6. Average percentage of true positive over $N_r = 300$ realizations with 4 sources, according to the number of sensors selected for our approach (blue line), SelRand (red line), SelGen (magenta plus) and SelRelax (black crosses). $\mathbf{A}_{\mathcal{K}}$ is defined for reflection of the (a) 3-rd, (b) 2-nd, (c) 1-st and (d) 0-th order. (color online)

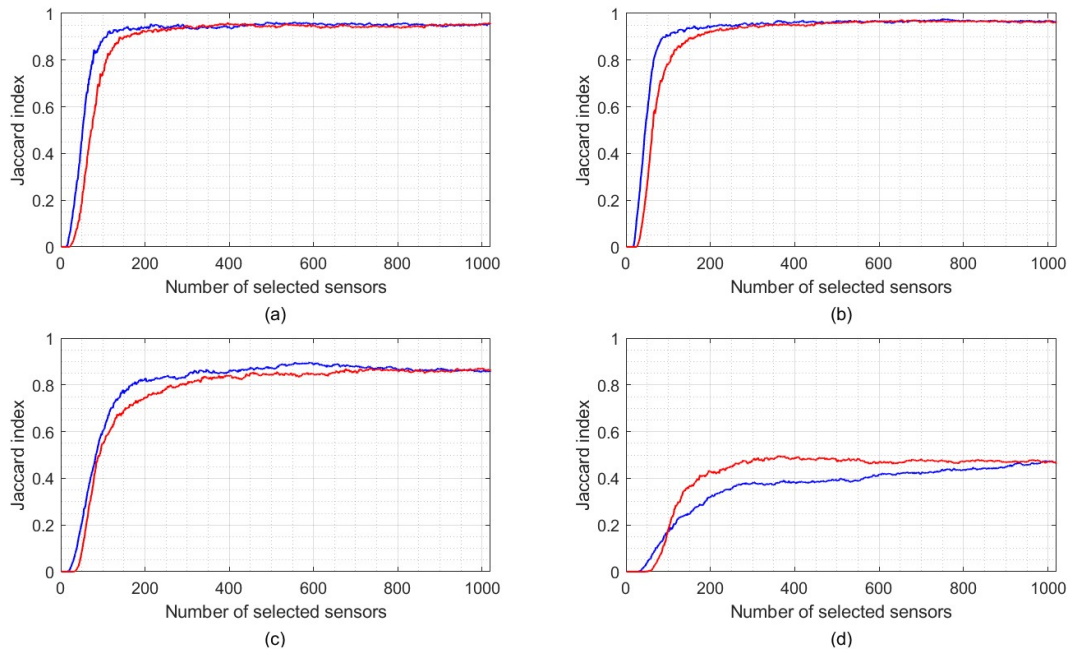


FIG. 7. Jaccard index over $N_r = 300$ realizations with 4 sources, according to the number of sensors selected for our approach (blue line) and SelRand (red line). $\mathbf{A}_{\mathcal{K}}$ is defined for reflection of the (a) 3-rd, (b) 2-nd, (c) 1-st and (d) 0-th order. (color online)

that the mirror-source model is more accurate. This correlation seems to be maximized at the 2-nd order, and slightly decays back beyond.

1. Performance analysis

Based on the results in table I and to fit with the graphs of sec. VIA, we display in the following the results with $\mathbf{A}_{\mathcal{K}}$ built for orders from 3 to 0. The plots are given in fig. 6.

One can note that the results considering 3 or 2 reflections are similar, which is in line with the correlation coefficient table I. We suggest that this similarity could occur because the mirrored sources beyond the 2-nd order do not contribute to improve the source localization as we could expect. It can also be thought that other model mismatches (such as wall positions and orientations, exact source positions, etc.) affect the source-mirror model beyond a given order. Surprisingly, regarding of all methods, the performance trends reveal that the studied mismatch has a lower impact in the present real scenario. Finally, apart from the model with no reflection, our proposed method leads to better results than the ones from the state-of-the-art. Again, the Jaccard index is plotted in the fig. 7, with a focus on the iterative selections only. Similarly to the simulation results, the Jaccard index is similar to the True positive rate with the 2-nd and 3-rd reflection order models. The difference is marginal with 1-st order, but becomes significant with the free field model. Again, this difference indicates a presence of False positives or False negatives that degrades the effective performance of source localization.

In addition to the previous Monte Carlo analysis, the fig. 8 provides an illustration of source localization results in one specific realization. It shows the absolute values of source vectors $\tilde{\mathbf{s}}_{\mathcal{K}}$, estimated with the different methods, with $S = 4$ sources, $K = 50$ sensors, and a model with the 3-rd order of reflection. The red dots correspond to the true source positions, the black ‘+’ (resp. ‘x’) signs provide the estimated source locations when they are true positives (resp. false positives). These figures reveal a sparse structure as expected, even if they do not contain 4 non-zero peaks only (then it can eventually leads to false positives). Our method (fig. 8(a)) appears to be the most sparse. Although these maps are specific to one realization, we verified that these observations remain true for any other one.

2. Statistical analysis of the selected sensors

This last section investigates if there are recurring patterns of selection in the different Monte Carlo realizations. In other words, one may wonder whether some sensors of the array are more *important* than others, regarding the information they provide. Indeed, the proposed selection is data-informed and depends on each specific realization, *i.e.* the source positions. Nevertheless, does the selection prioritize some sensors more often in average?

This question naturally leads to analyze the probability that the k -th sensor is selected among the r first ones. As such, it relates with the following empirical cumulative distribution (cdf):

$$\mathcal{P}(\mathbf{p}_k \in \mathcal{K}; |\mathcal{K}| \leq r). \quad (27)$$

Obviously, this probability monotonically increases since it is a cdf, and is defined for $2 \leq r \leq M$.

The fig. 9 draws this empirical cdf for each of the $M = 1020$ sensors. It evidences that cdfs are heterogeneous, and reach 1 at a different rate according to the sensor index k . Consequently, some sensors are more likely to be selected than others to create an array of r (or less) elements. To illustrate this, we display in fig. 10, the 60 sensors having the highest values $\mathcal{P}(\mathbf{p}_k \in \mathcal{K}; |\mathcal{K}| \leq r)$ for $r = 50$, and the color indicates the corresponding value. Interestingly, most of these sensors lie in the plane in which the sources belong to.

Remark At this point, the statistical study indeed reveals recurring selection patterns in the different realizations. One intuition would be to extract the most appearing sensors to design *one* global array. In this way, array design could be done once and *offline* for a realistic scenario, thanks to the proposed *online* sensor selection performed on a set of simulated data. Although beyond the scope of this paper, it seems to be an interesting future investigation.

VII. DISCUSSION AND OPEN PROBLEMS

With this paper, the authors wish to initiate the investigation of source localization helped by iterative sensor selection. The presented work experimentally validates the interest of this research direction, however some problems remain open.

First, the stopping criterion of the algorithm 1 is a chosen sensor number K . In practice, this remains a limitation because K may be too small to reach the asymptotic performance obtained when $K = M$. It also may be chosen too large, so that the addition of the latest sensors brings a marginal improvement on the source location estimation. Thus, an alternative stopping criterion based on an automatic choice of K is a future direction to investigate in order to enhance the use of the algorithm.

The second open problem deals with the computation time. Indeed, SBL needs to be repeated K times, and has a complexity of order $\mathcal{O}(|\mathcal{K}| \cdot N^2)$ ⁴⁵. If $K \approx M$ it is trivial that the iterative approach requires more computation than doing SBL once with the full array. Nevertheless, the computation time of the algorithm 1 is generally more time-consuming, since the dimension of the source vector N mainly drives the complexity of SBL. Replacing the conventional SBL with an accelerated technique of lower complexity is consequently one interesting direction to explore – see for example the state of the art introduction in²⁹.

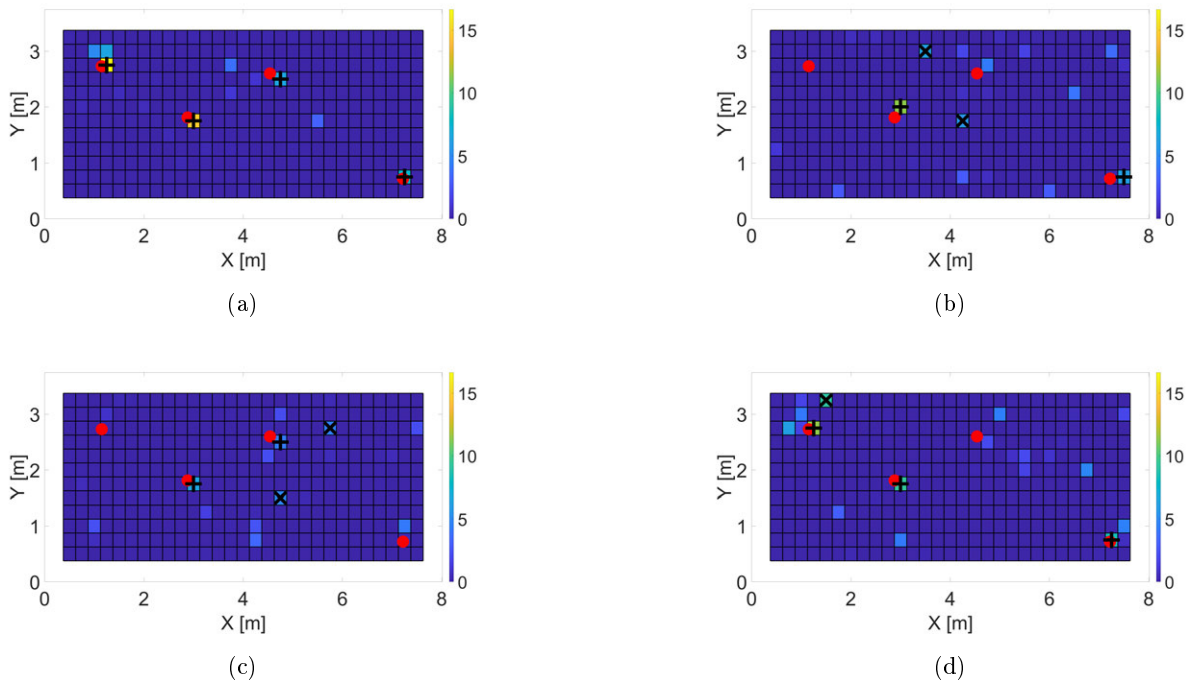


FIG. 8. Source localization estimation done by SBL $\tilde{\mathbf{s}}_{\mathcal{K}}$ for 1 realization, with $S = 4$ sources and $K = 50$ sensors. (a) Proposed approach, (b) SelRand, (c) SelGen, (d) SelRelax. (color online)

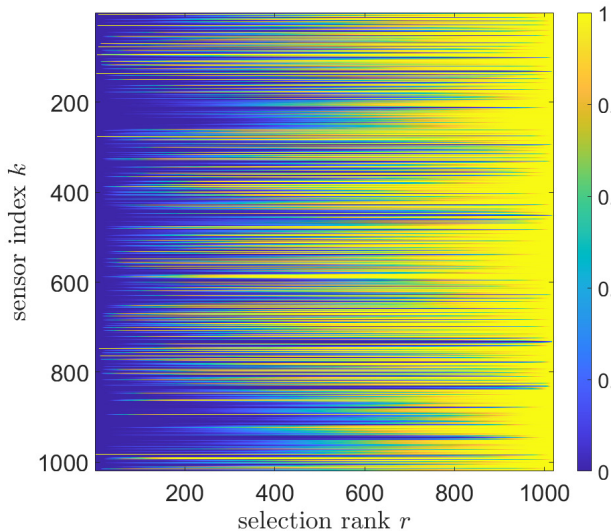


FIG. 9. Cumulative distribution function (27) of the $M = 1020$ sensors, for $0 \leq r \leq 1020$. (color online)

VIII. CONCLUSION

In this paper, a greedy sensor selection approach is proposed, with a view to performing sparse acoustic source localization with a limited number of sensors. The approach relies on the D-optimal design in the Bayesian

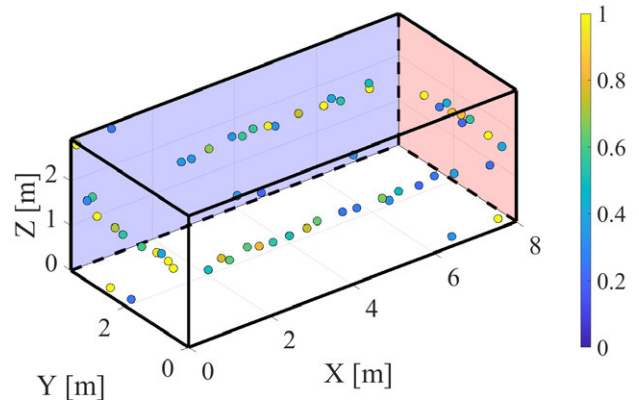


FIG. 10. cdf values (27) for $r = 50$, at corresponding sensor locations. For sake of clarity, we only display the 60 highest values. (color online)

framework, and enables the selection procedure to be *online*. The method alternates between source localization given the selected sensors, and a selection of the most informative sensor candidate given the source localization covariance.

The performance analysis encompasses both numerical and experimental validations, in an acoustic indoor scenario. The comparison with different state-of-the-art methods shows that the proposed approach generally per-

forms better. An empirical study of the sensor selection robustness to model mismatch is also presented. In the studied scenario, choosing a reliable mirror source model is challenging for indoor source localization, especially concerning the choice of the reflection order. Interestingly, the proposed online approach is more robust to this given mismatch than the compared state-of-the-art methods. The origin of this observed robustness need further investigations towards a more theoretical comprehension.

Finally, further works could investigate how to tackle offline microphone array design, based on the proposed online sensor selection with synthesized data. This idea, suggested in sec. [VIB 2](#), would open possibilities to microphone array design.

IX. ACKNOWLEDGMENTS

This work is supported by DGA (Direction Générale de l'Armement). The authors wish to thank the d'Alembert Institute (Sorbonne Université), and especially François Ollivier and Hugo Demontis, for giving access to their experimental facilities.

- ¹Allen, J. B., and Berkley, D. A. (1979). "Image method for efficiently simulating small-room acoustics," *The Journal of the Acoustical Society of America* **65**(4), 943–950, <https://asa.scitation.org/doi/10.1121/1.382599>, doi: [10.1121/1.382599](https://doi.org/10.1121/1.382599).
- ²Antoni, J. (2012). "A bayesian approach to sound source reconstruction: optimal basis, regularization, and focusing," *The Journal of the Acoustical Society of America* **131**(4), 2873–2890.
- ³Boeringer, D. W., and Werner, D. H. (2004). "Particle swarm optimization versus genetic algorithms for phased array synthesis," *IEEE Transactions on antennas and propagation* **52**(3), 771–779.
- ⁴Boyd, S., and Vandenberghe, L. (2004). *Convex Optimization* (Cambridge University Press, USA).
- ⁵Brooks, T. F., and Humphreys, W. M. (2006). "A deconvolution approach for the mapping of acoustic sources (DAMAS) determined from phased microphone arrays," *Journal of Sound and Vibration* **294**(4), 856–879.
- ⁶Chardon, G., Daudet, L., Peillot, A., Ollivier, F., Bertin, N., and Gribonval, R. (2012). "Nearfield acoustic holography using sparsity and compressive sampling principles," *The Journal of the Acoustical Society of America* **132**(3), 1152–1534, doi: [10.1121/1.4740476](https://doi.org/10.1121/1.4740476).
- ⁷Chepuri, S. P., and Leus, G. (2014). "Sparsity-promoting sensor selection for non-linear measurement models," *IEEE Transactions on Signal Processing* **63**(3), 684–698.
- ⁸Cover, T. M., and Thomas, J. A. (2006). *Elements of Information Theory (Wiley Series in Telecommunications and Signal Processing)* (Wiley-Interscience, New York, NY, USA).
- ⁹Cox, H., Zeskind, R., and Owen, M. (1987). "Robust adaptive beamforming," *IEEE Transactions on Acoustics, Speech, and Signal Processing* **35**(10), 1365–1376.
- ¹⁰Demontis, H., Ollivier, F., and Marchal, J. (2018). "3d identification of acoustic sources in rooms using a large-scale microphone array," in *2018 16th International Workshop on Acoustic Signal Enhancement (IWAENC)*, IEEE, pp. 506–509.
- ¹¹Demontis, H., Ollivier, F., and Marchal, J. (2019). "Block-sparse approach for the identification of complex sound sources in a room," in *EAA Spatial Audio Signal Processing Symposium*, pp. 13–17.
- ¹²Ding, J., and Zhou, A. (2007). "Eigenvalues of rank-one updated matrices with some applications," *Applied Mathematics Letters* **20**(12), 1223–1226, doi: [10.1016/j.aml.2006.11.016](https://doi.org/10.1016/j.aml.2006.11.016).
- ¹³Federer, W. r. (1956). *Experimental design*, **81** (LWW).
- ¹⁴Gaumond, C. F., and Edelmann, G. (2013). "Application of statistical reduced isometry property to design of line arrays for compressive beamforming," in *Proceedings of Meetings on Acoustics*, Acoustical Society of America, Vol. 19, p. 070083.
- ¹⁵Gemba, K. L., Nannuru, S., and Gerstoft, P. (2019). "Robust ocean acoustic localization with sparse bayesian learning," *IEEE Journal of Selected Topics in Signal Processing* **13**(1), 49–60.
- ¹⁶Gemba, K. L., Nannuru, S., Gerstoft, P., and Hodgkiss, W. S. (2017). "Multi-frequency sparse bayesian learning for robust matched field processing," *The Journal of the Acoustical Society of America* **141**(5), 3411–3420.
- ¹⁷Gerstoft, P., Mecklenbräuker, C. F., Xenaki, A., and Nannuru, S. (2016). "Multisnapshot sparse bayesian learning for DOA," *IEEE Signal Processing Letters* **23**(10), 1469–1473, doi: [10.1109/LSP.2016.2598550](https://doi.org/10.1109/LSP.2016.2598550).
- ¹⁸Gilquin, L., Lecomte, P., Antoni, J., Le Magueresse, T., and Marteau, C. (2020). "Iterative positioning of microphone arrays for acoustic imaging," *Journal of Sound and Vibration* **469**, 115116.
- ¹⁹Grant, M., and Boyd, S. (2014). "CVX: Matlab software for disciplined convex programming, version 2.1" <http://cvxr.com/cvx>.
- ²⁰Haupt, R. (1994). "Thinned arrays using genetic algorithms," *IEEE Transactions on Antennas and Propagation* **42**(7), 993–999, doi: [10.1109/8.299602](https://doi.org/10.1109/8.299602).
- ²¹Herzet, C., and Drémeau, A. (2010). "Bayesian pursuit algorithms," in *EURASIP European Signal Processing Conference, EUSIPCO*.
- ²²Herzet, C., and Drémeau, A. (2010). "Sparse representation algorithms based on mean-field approximations," in *IEEE International Conference on Acoustics, Speech and Signal Processing, ICASSP*.
- ²³Jensen, F. B., Kuperman, W. A., Porter, M. B., and Schmidt, H. (2011). *Modern Acoustics and Signal Processing Computational Ocean Acoustics*, 2 ed. (Springer-Verlag, New York), <https://www.springer.com/gp/book/9781441986771>.
- ²⁴Ji, S., Xue, Y., and Carin, L. (2008). "Bayesian compressive sensing," *IEEE Transactions on signal processing* **56**(6), 2346–2356.
- ²⁵Joshi, S., and Boyd, S. (2008). "Sensor selection via convex optimization," *IEEE Transactions on Signal Processing* **57**(2), 451–462.
- ²⁶Khodier, M., and Christodoulou, C. (2005). "Linear array geometry synthesis with minimum sidelobe level and null control using particle swarm optimization," *IEEE Transactions on Antennas and Propagation* **53**, 2674–2679, doi: [10.1109/TAP.2005.851762](https://doi.org/10.1109/TAP.2005.851762).
- ²⁷Krause, A., Singh, A., and Guestrin, C. (2008). "Near-optimal sensor placements in gaussian processes: Theory, efficient algorithms and empirical studies," *Journal of Machine Learning Research* **9**(2).
- ²⁸Le Courtois, F., Pascal, J.-C., Thomas, J.-H., and Poisson, F. (2010). "Optimisation par algorithme génétique de la géométrie d'antenne pour la localisation de sources," in *10ème Congrès Français d'Acoustique*.
- ²⁹Lin, A., Song, A. H., Bilgic, B., and Ba, D. (2022). "Covariance-free sparse bayesian learning," *IEEE Transactions on Signal Processing*.
- ³⁰Liu, W., Gao, W.-c., Sun, Y., and Xu, M.-j. (2008). "Optimal sensor placement for spatial lattice structure based on genetic algorithms," *Journal of Sound and Vibration* **317**(1-2), 175–189.
- ³¹Murino, V., Trucco, A., and Regazzoni, C. (1996). "Synthesis of unequally spaced arrays by simulated annealing," *IEEE Transactions on Signal Processing* **44**, 119–122, doi: [10.1109/78.482017](https://doi.org/10.1109/78.482017).
- ³²Pukelsheim, F. (2006). *Optimal design of experiments* (SIAM).
- ³³Ranieri, J., Chebira, A., and Vetterli, M. (2014). "Near-optimal sensor placement for linear inverse problems," *IEEE Transactions on Signal Processing* **62**(5), 1135–1146, doi: [10.1109/TSP.2014.2299518](https://doi.org/10.1109/TSP.2014.2299518).

- ³⁴Ribeiro, F., Zhang, C., Florêncio, D. A., and Ba, D. E. (2010). “Using reverberation to improve range and elevation discrimination for small array sound source localization,” *IEEE Transactions on Audio, Speech, and Language Processing* **18**, 1781–1792, doi: [10.1109/TASL.2010.2052250](https://doi.org/10.1109/TASL.2010.2052250).
- ³⁵Schniter, P., Potter, L. C., and Ziniel, J. (2008). “Fast Bayesian matching pursuit,” in *IEEE Information Theory and Applications Workshop*, pp. 326–333.
- ³⁶Seeger, M., Nickisch, H., Pohmann, R., and Schölkopf, B. (2010). “Optimization of k-space trajectories for compressed sensing by bayesian experimental design,” *Magnetic Resonance in Medicine: An Official Journal of the International Society for Magnetic Resonance in Medicine* **63**(1), 116–126.
- ³⁷Seeger, M. W., and Nickisch, H. (2008). “Compressed sensing and bayesian experimental design,” in *Proceedings of the 25th international conference on Machine learning*, pp. 912–919.
- ³⁸Soussen, C., Idier, J., Brie, D., and Duan, J. (2011). “From Bernoulli–Gaussian Deconvolution to Sparse Signal Restoration,” *IEEE Transactions on Signal Processing* **59**(10), 4572–4584, doi: [10.1109/TSP.2011.2160633](https://doi.org/10.1109/TSP.2011.2160633).
- ³⁹Tipping, M. E. (2001). “Sparse bayesian learning and the relevance vector machine,” *Journal of machine learning research* **1**(Jun), 211–244.
- ⁴⁰Trucco, A. (1999). “Thinning and weighting of large planar arrays by simulated annealing,” *IEEE Transactions on Ultrasonics, Ferroelectrics, and Frequency Control* **46**, 347–355, doi: [10.1109/58.753023](https://doi.org/10.1109/58.753023).
- ⁴¹Van Veen, B. D., and Buckley, K. M. (1988). “Beamforming: A versatile approach to spatial filtering,” *IEEE assp magazine* **5**(2), 4–24.
- ⁴²Wynn, H. P. (1970). “The sequential generation of d-optimum experimental designs,” *The Annals of Mathematical Statistics* **41**(5), 1655–1664.
- ⁴³Xenaki, A., Gerstoft, P., and Mosegaard, K. (2014). “Compressive beamforming,” *The Journal of the Acoustical Society of America* **136**(1), 260–271.
- ⁴⁴Yan, K.-K., and Lu, Y. (1997). “Sidelobe reduction in array-pattern synthesis using genetic algorithm,” *IEEE Transactions on Antennas and Propagation* **45**(7), 1117–1122.
- ⁴⁵Yang, Z., Xie, L., and Zhang, C. (2012). “Off-grid direction of arrival estimation using sparse bayesian inference,” *IEEE Transactions on Signal Processing* **61**(1), 38–43.
- ⁴⁶Zayyani, H., Babaie-Zadeh, M., and Jutten, C. (2008). “Decoding real field codes by an iterative Expectation-Maximization (EM) algorithm,” in *IEEE International Conference on Acoustics, Speech and Signal Processing, ICASSP*.